RSC Advances




ROYAL SOCIETY OF CHEMISTRY

www.rsc.org/advances

# Graphical Abstract

**Table of contents entry:**

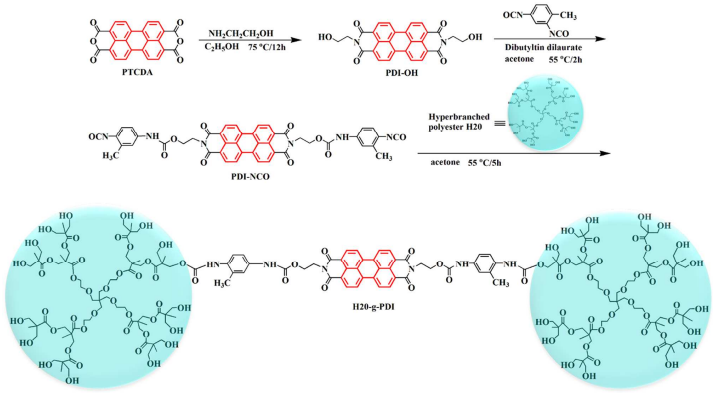


**Highlight**

The mechanical and thermal properties of epoxy were significantly enhanced modified by H20-g-PDI.

RSC Advances RSCPublishing

ARTICLE

# Enhanced mechanical and thermal properties of epoxy with hyperbranched polyester grafted perylene diimide

Cite this: DOI: 10.1039/x0xx00000x

Received 00th xxxx 201x
Accepted 00th xxxx 201x

DOI: 10.1039/x0xx00000x

www.rsc.org/

Lulu Pan[1], Shaorong Lu*[1], Xiane Xiao[1], Zihai He[1], Cen Zeng[1], Jian Gao[1], Jinhong Yu*[1,2]

A new kind of reactive toughening agent, named H20-g-PDI, have been successfully synthesized via hyperbranched polyester (H20) grafted to perylene diimide (PDI). The chemical structure of H20-g-PDI were characterized by Fourier transformed infrared spectroscopy (FT-IR), differential scanning calorimetry (DSC), wide angle X-ray diffractometry (WAXD), respectively. The H20-g-PDI was used as toughening agents to enhance the mechanical and thermal properties of epoxy resin. The morphology, mechanical and thermal properties of the composites were systematically investigated. The experimental results revealed that the impact strength, tensile strength, flexural strength and flexural modulus of the epoxy resin modified by H20-g-PDI reached the highest value of 47.6 KJ/m$^2$, 93.19 MPa, 128.8 MPa, and 2205 MPa, respectively. These were 81.33%, 68.1%, 62.0%, and 19.8% higher than that of the neat epoxy when the content of H20-g-PDI loading reached 1.5 wt%. In addition, the glass transition temperature ($T_g$) and thermal stability of the epoxy composites also enhanced. $T_g$ and the decomposition temperature ($T_d$) of the epoxy composites were about 20 $^o$C and 27 $^o$C higher than those of neat epoxy, respectively. It is suggested that the formation of H20-g-PDI is effective to enhance the mechanical and thermal properties due to the homogeneous dispersion and strong interaction between the H20-g-PDI and epoxy matrix.

## 1. Introduction

Over the last decades, perylene diimide (PDI) acting as a derivative of 3, 4, 9, 10-perylene tetracarboxylic anhydride (PTCDA), has been attracted considerable attention not only in academic but also in industrial dye and pigment research due to their strong $\pi$-$\pi$ interaction force among the molecules. PDI has a great deal of lattice energy and large rigidity because of benzene ring plane conjugate structure. [1-4]. Usually, PDI derivatives has been widely applied such as in dye, *n*-type semiconductor materials and biological fluorescent field [5,6]. Different types of intermolecular forces such as hydrogen bonding and $\pi$-$\pi$ stacking interactions have been applied to direct the formation of desirable supramolecular structures of PDIs. And PDIs can be modified through introducing different groups onto the location of bay or imide [7,8]. For example, a long chain segment can reduce its rigidity in order to achieve the purpose of improving its performance [9]. Based on these, it possesses outstanding chemical and thermal stabilities [5], which are contributed to the thermal stability of modified thermosetting epoxy resin.

Epoxy resins are well-known to exhibit excellent mechanical properties, good thermal stability and strong adhesion performance. Epoxy resins have been widely applied in electronic-packaging materials, adhesives, reactive diluents, and vacuum pressure impregnation of coils, et al. [10-12]. However, the poor resistance to crack propagation and the inherent brittleness lead to the effective usage of epoxy resin as structural composites is restricted. Hence, the epoxy resins applications required high toughness [13,14]. To our best knowledge, numerous of studies had been worked on improving the properties of epoxy resins. This problem has been solved by using secondary components such as rubbers of low molecular weight，rigid component or crosslinked polymer [15]. The methods modifying fracture toughness of epoxy resin are invariable. Meanwhile, adding inorganic powders, such as silica and alumina have improved the toughness of epoxy without sacrificing their intrinsic properties, but the viscosity is increases with the increment of inorganic powders [16,17]. Hence, much work has been made to modify epoxy through adding secondary components such as highly

[1]*Key Laboratory of New Processing Technology for Nonferrous Metals and Materials, Ministry of Education, School of Material Science and Engineering, Guilin University of Technology, Guilin 541004, China.*

[2]*Key Laboratory of Marine New Materials and Application Technology, Zhejiang Key Laboratory of Marine Materials and Protection Technology, Ningbo Institute of Material Technology & Engineering, Chinese Academy of Sciences, Ningbo, 315201, China. Email address:* ***lushaor@163.com (S.R. Lu); yujinhong@glut.edu.cn (J.H. Yu).***

hyperbranched polymers (HBP) [18,19]. Generally, epoxy resins modified with polyimide or polyester through chemical reactions or physical blending method has been reported to enhance the thermal stability and good mechanical properties of epoxy resins [20].

Hyperbranched polymers have densely branched structures and numbers of end-groups, which possess excellent flow and processing properties [21,22]. Recently, Hyperbranched polymers, especially polyesters, have been considered as a novel and intriguing modifiers for brittle epoxy resins, which can effectively improve the mechanical properties [23,24]. Due to possessing lower viscosity, hyperbranched polymers ended with hydroxy or carboxyl groups have better processability [25]. In comparison with other hyperbranched polymer, the hyperbranched polyester (H20) which contains higher density hydroxyls grafted on the surface can increase the interfacial forces between the hyperbranched polyester and the epoxy network [26,27]. Three-dimensional networks of epoxy system contain a plenty of unoccupied spaces, and will increase with the increment of H20. In this way, the free volume of cured epoxy becomes larger, resulting in the flexibility of chain segments [28,29]. The polyesters are effective to improve toughness without sacrificing stiffness and glass temperature [30,31].

In this study, a new kind of reactive toughening agent denoted as H20-g-PDI was first synthesized in order to enhance the mechanical and thermal properties of epoxy. The H20-g-PDI is ended with hydroxyl group which can react with epoxy resins and form crosslinking networks leading to high crosslinking density during curing reaction. The effect of the H20-g-PDI on mechanical and thermal properties of the epoxy composite was investigated. It is suggested that the formation of H20-g-PDI could contributed to modify epoxy and improve the properties, which is useful for the fundamental research and real applications.

# 2. Experimental

### 2.1. Materials

3, 4, 9, 10-perylene tetracarboxylic anhydride (PTCDA) was obtained from Xiya Chemical Reagent Company (Chengdu, China). The hyperbranched aliphatic polyester BoltornTM (H20) was provided by Perstorp AB company (Sweden) and used directly. 2-aminoethanol (AE) was supplied by Xilong Chemical Reagent Co., Ltd., China. Diglycidylether of bisphenol A (DGEBA) epoxy resin E-44 (with an epoxide equivalent weight of 227 g/mol) was purchased from Yueyang Chemical Plant in China. 4,4'-diaminodiphenylsulphone (DDS) and toluene-2,4-diisocyanate (TDI) were obtained from Sinopharm Chemical Reagent Co., Ltd., China. Di-n-butyltindilaurate (DBTDL) was used as a catalyst. Acetone was first dried with calcium hydride and then distilled before using. All other reagents and solvents were used as received without further purification.

### 2.2. Synthesis of the perylene diimde derivatives (PDI-OH)

The synthetic route of the PDI-OH was shown in **Scheme 1** [32]. The experimental details were described as follows: 3, 4, 9, 10-perylene tetracarboxylic anhydride (PTCDA) (1.5 g, 3.1 mmol) and anhydrous ethanol (80 ml) were added into a 250 ml round-bottomed three-neck flask equipped with nitrogen inlet and thermometer. Then the solution was stirred for 30 min, and then introduced 2-aminoethanol in it. The mixture was further stirring at 75 °C for 12 h under nitrogen. After that, ethanol was removed and the final product was precipitate with deionized water. Then collected by filtration and the filter residue was washed with 3% KOH aqueous solution several times under ultrasonic oscillation for 10 min in order to remove the unreacted PTCDA. At last, the solid was washed with distilled water to remove the potassium hydroxide, then dried at 60 °C under vacuum drying oven to give a red brown powder (yield: 74%).

### 2.3. Preparation of hyperbranched polyester (H20) grafted perylene diimde derivatives (H20-g-PDI)

The experimental details of H20-g-PDI were described as follows: PDI-OH (0.2 g, 0.35 mmol) and anhydrous acetone (10 ml) were placed in a 250 ml dried three-necked flask and dispersed through ultrasonic oscillation for 10 min. A few drops of di-n-butyltindilaurate (DBTDL) were added to the mixture, and then heated to 55 °C for 15 min under a nitrogen atmosphere. Then mixture of TDI (1 mmol) and acetone (2 ml) was slowly dropped into the above-mentioned mixture and stirred at 55 °C for 2 h. Thus, the intermediate product with isocyanate group, denoted as PDI-NCO was successful synthesized. H20 (1.7 g, 1mmol) was dissolved in acetone before reaction and added to the PDI-NCO mixed solution. The solution reacted at 55 °C for 5 h. After temperature was cooled to room temperature, the solution poured into distilled water to precipitate, filter and wash with ethanol several times. Finally, H20-g-PDI was dried in vacuum drying oven at 80 °C for 24 h. Typical procedure of preparing H20-g-PDI is described as **Scheme 1**.

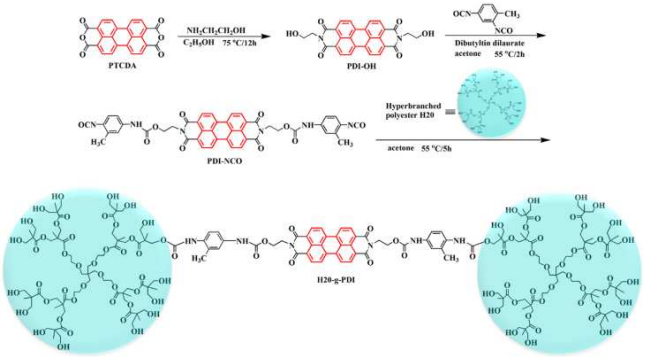


**Scheme 1** The preparation process of H20-g-PDI.

### 2.4. Preparation of H20-g-PDI/epoxy composites

The H20-g-PDI/epoxy composites were prepared as follows: firstly, an equivalent of H20-g-PDI was first dispersed in acetone through ultrasonic for 10 min, then 26.0 g epoxy resin was poured. Secondly, the temperature increased to 60 °C and mixture was stirred for 1 h to ensure good homogeneity and remove the acetone entirely. DDS (30 g/100 g of epoxy resin) was added acting as curing agent under vigorous mechanical stirring. Subsequently, the solution was degassed at 120 °C for 30 min. Finally, the mold was placed in a convection oven to cure at 140 °C for 2 h, 160 °C for 2 h and 180 °C for 2 h. Different weight fractions (0, 0.5, 1.0, 1.5 and 2.0 wt%) of samples were prepared by above methods. The details of the preparation of the epoxy composites are shown in **Scheme 2**.

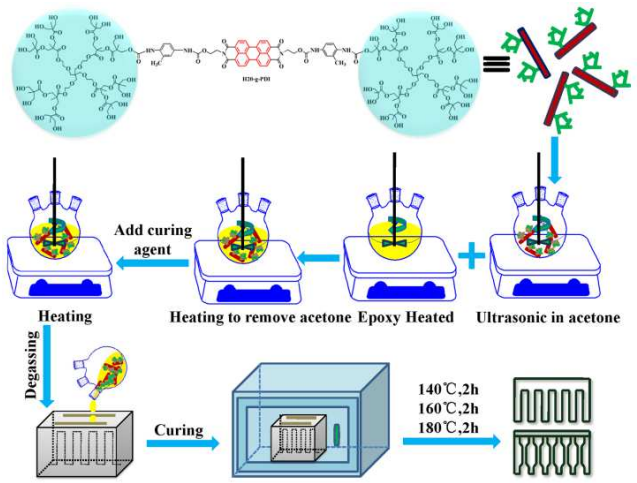


**Scheme 2** The preparation process of the epoxy composites.

### 2.5. Characterization

Fourier transform infrared spectra (FT-IR) was recorded using Perkin-Elmer 1710 spectrophotometer at a resolution of 4 $cm^{-1}$ with 32 scans over the range of 4000-500 $cm^{-1}$. Wide angle X-ray diffraction (WAXD) measurement was performed by D8 ADVANCE X-ray diffractometer and the scanning range ranges from 5° to 60° at a speed of 2° $min^{-1}$. Thermogravimetric analysis (TGA) instrument (NETZSCH STA-449) was used to probe the thermal stability up to 800 °C at a scanning rate of 10 °C$min^{-1}$. And all samples were performed under nitrogen atmosphere with the sample weight of about 3 mg. Differential scanning calorimetry (NETZSCH DSC-204) of epoxy composites was performed at temperatures from 50 to 250 °C at a heating rate of 20 °C$min^{-1}$ under nitrogen atmosphere. Morphology of the specimens were observed by field emission scanning electron microscopy (FE-SEM) on a JEOL JSM-6610 instrument at an accelerating voltage of 30 kV, and the fracture surfaces were coated with sputter-gold to improve the conductivity. Dynamic mechanical analysis (DMA) was performed with a TA Instruments (DMA Q800 dynamic mechanical analyzer) made in USA to determine modulus and glass transition temperature ($T_g$). And the test was performed from 40 to 250 °C at a heating rate of 3 °C$min^{-1}$ under nitrogen atmosphere. Mechanical properties of the composites were evaluated by impact, tensile and flexural measurements. The impact strength of the cured samples was measured with a tester of type XJJ-5, which has no notch in the specimen according to National Standard of China (GB1043-79). And the cured specimen's size was trimmed into a dimension of 80×10×4 mm for measuring the mechanical properties. The tensile strength was examined on a universal tensile tester of type RGT-5 according to National Standard of China (GB1040-92) at a rate of 2 mm·$min^{-1}$. Flexural tests were performed by WDW-20 (Shenzhen Jun Red Instrument Equipment Co., Ltd, China) according to a three-point bending mode of the universal testing machine at a crosshead speed of 2 mm·$min^{-1}$. The conditions of the tests and the specimens conformed to GB1449-2005. The test results are the average value of five specimens and the testing temperature was room temperature.

## 3. Results and discussion

### 3.1. Characterization of H20-g-PDI

The FT-IR spectra of PTCDA, PDI-OH, PDI-NCO and H20-g-PDI are shown in **Fig. 1**. For the PTCDA, the sharp peak at 1773 $cm^{-1}$ is attributed to C=O of the ester group indicating the reaction between perylene and 2-aminoethanol. The FT-IR spectrum of PDI-OH exhibits characteristic absorption bands at 3105 $cm^{-1}$ (aromatic C-H stretching), 2958 $cm^{-1}$ and 2889 $cm^{-1}$ (aliphatic C-H stretching), 1689 $cm^{-1}$ and 1660 $cm^{-1}$ (imide C=O stretching), 1592 $cm^{-1}$ (conjugated C=C stretching), 1344 $cm^{-1}$ (C-N stretching), 1177 $cm^{-1}$ ($CH_2$-O stretching), 810 $cm^{-1}$ and 743 $cm^{-1}$ (C-H bending). And the peaks at 3446 $cm^{-1}$ and 3359 $cm^{-1}$ are characteristic of -OH and urethane N-H stretching, respectively [33]. Several new peaks were observed in the FT-IR spectrum of the PDI-NCO. A sharp and typical absorption peak appeared at 2270 $cm^{-1}$ that can be attributed to the isocyanate functional group of the PDI-NCO [34]. And the band at 3409 $cm^{-1}$ can be explained to overlap between free hydrogen bond and N-H stretching. For the spectrum of H20-g-PDI, the absence of isocyanate stretching band at 2270 $cm^{-1}$ also evidence completion of the reaction between hydroxyl and diisocyanate. The wide absorptions at 3419 $cm^{-1}$ belong to the urethane N-H stretch. The distinct and wide peak at 3419 $cm^{-1}$ is attributed to the hydroxyl stretching vibration of H20 (Hyperbranched polyester). The band at 3300-3500 $cm^{-1}$ represents the overlapping of -OH and -NH stretching vibrations in the H20-g-PDI [35].

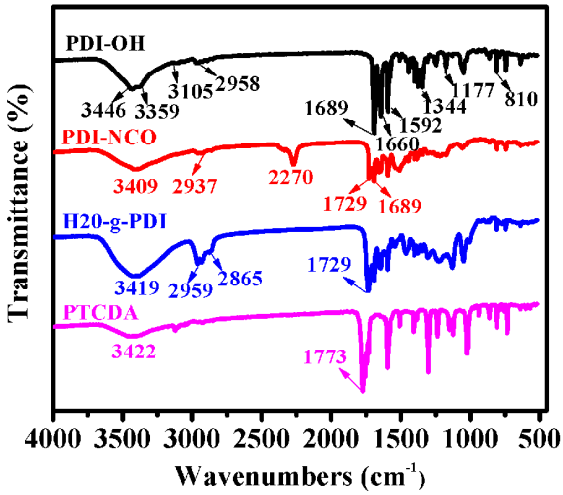


**Fig. 1** FT-IR spectra of PTCDA, PDI-OH, PDI-NCO and H20-g-PDI.

The TGA data of PTCDA, PDI-OH and H20-g-PDI are listed in **Fig. 2**. It can be seen from **Fig. 2a**, the weight loss of the PTCDA at 700 °C is 43.9% [36]. It suggested that PTCDA has high decomposition temperature owing to the rigid construction. Comparing to the PTCDA, the curve PDI-OH shows two decomposition platforms. The first platforms is at 527 °C, which is attributed to the loss of alkyl chain segment belongs to ethanolamine moieties in the molecule, indicated that the addition of alkyl chain segment could reduce the decomposition temperature [37]. Similar to the PTCDA, the second decomposition platform was the final decomposition temperature, which was the decomposition of benzene ring of the perylene diimde. The weight loss of PDI-OH is stabilized at 48.4% at 700 °C. As can be seen from the curve H20-g-PDI (**Fig. 2a**), the thermostability of the H20-g-PDI is less stable comparing to the PTCDA's. The first decomposition

temperature is at 215 °C owing to the decomposition of urethane bond [38]. The decomposition temperature at 10% weightlessness (designated as $T_{10}$) of H20-g-PDI is lower than that of PDI-OH. The low decomposition temperature overcomes difficult processing problem of the PTCDA. The $T_{10}$ occurs differently as shown in **Table 1**. From TGA curves, the decomposition of H20-g-PDI shows a different pathway comparing to PTCDA and PDI-OH, which indicates that H20 is indeed grafted to the intermediate product [39]. DTG curves were shown in **Fig. 2b**. The temperatures at the maximum weight loss rate ($T_{max}$) are seen from the peak values of the DTG curves. The $T_{max}$ of the PTCDA is at 605 °C and the PDI-OH shifts the maximum value to 527 °C, which reduced by 78 °C owing to the addition of ethanolamine. However, the $T_{max}$ of the H20-g-PDI decrease obviously to 300 °C, which reduced by 227 °C comparing to PDI-OH. All of these changes indicated that the H20 was successfully grafted to the intermediate product of PDI-NCO.

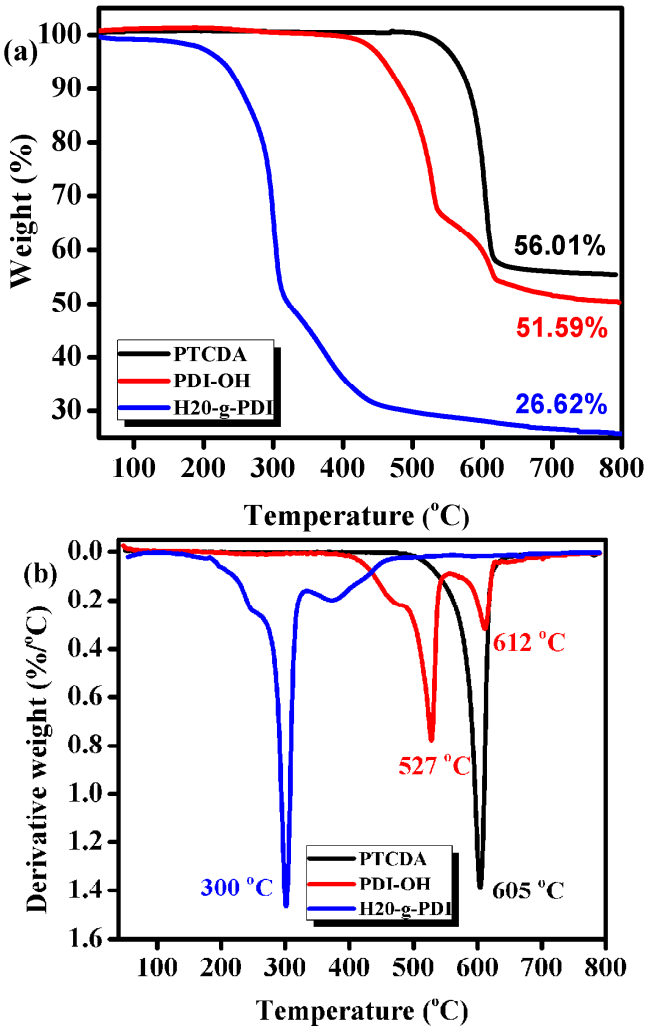


**Fig. 2** TGA curves (a) and DTG curves (b) of PTCDA, PDI-OH and H20-g-PDI.

The wide-angle X-ray diffraction curves of PTCDA, PDI-OH, and H20-g-PDI are shown in **Fig. 3**. It can be seen that PTCDA spectra shows five strong peaks at $2\theta$ = 9.6°, $2\theta$ = 12.6°, $2\theta$ = 24.9°, $2\theta$ = 27.6° and $2\theta$ = 28.5°, indicating a high degree of crystallinity [40]. The products PDI-OH and H20-g-PDI also present the same diffraction peaks, to some extent. Compare to PTCDA, the intensity of the peaks were distinctly weakened. Illustrate that, PTCDA modified by 2-aminoethanol and H20 molecules only reduced the degree of crystallinity, the internal crystal structure unchanged. Moreover, for H20-g-PDI, a broad peak was displayed around 17.7°, which can be attributed to disordered alkyl chains [41]. According to the Bragg equation $2d\sin\theta = n\lambda$, the additional diffraction peak at $2\theta$ = 26° calculate the interplanar distance d = 0.34 nm, which is similar to other perylene diimides crystals (0.35 nm) [8,42]. This was attributed to the intermolecular π-π stack of perylene diimide [8]. But the intensity was very weak due to the hyperbranched structure decreases the crystallinity of products and increases its disorder [43]. Thus the wide-angle X-ray diffraction also proves H20 successfully modified PTCDA. Meanwhile, the optical photographs of PTCDA, PDI-OH and H20-g-PDI solution are shown in the inset of **Fig. 3**. PDI-OH and H20-g-PDI can be dispersed well in acetone because of the surface's hydroxyl groups.

**Table 1** Thermal data of the PTCDA, PDI-OH and H20-g-PDI under nitrogen atmosphere.

| Sample | $T_{10}$ (°C) | $T_{50}$ (°C) | $T_{max}$ (°C) | Calculated loading (at 700 °C) |
|---|---|---|---|---|
| PTCDA | 580.7 | 603.75 | 605 | 56.01% |
| PDI-OH | 483.7 | 529.64 | 527 | 51.59% |
| H20-g-PDI | 252.2 | 297.56 | 300 | 26.62% |

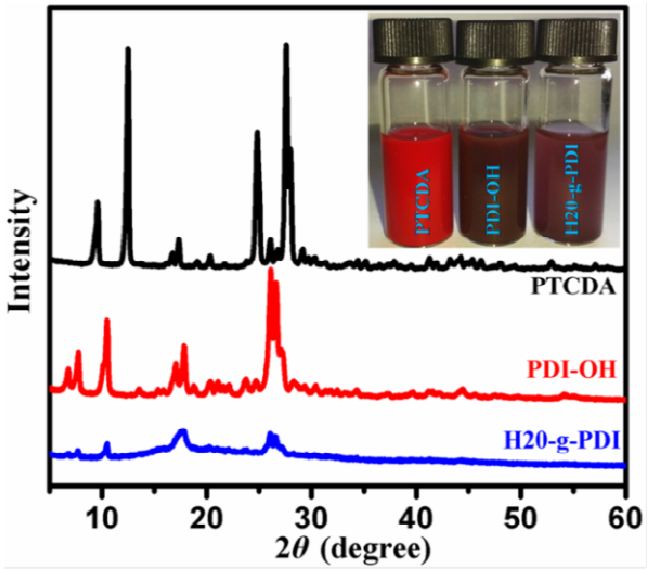


**Fig. 3** WAXD curves of PTCDA, PDI-OH and H20-g-PDI.

### 3.2. Morphology of composites

The microstructure and the interface properties of the composite have an important influence on the macro performance. The morphologies of the impact fracture surface of the neat epoxy and its composites are observed by SEM and presented in **Fig. 4**. As can be seen from **Fig. 4(a-b)** with different enlargement fractions, the fracture surface of the neat epoxy shows a relatively smooth surface except for several river-like lines and single crack propagation direction, which is shown as the arrow in the **Fig. 4(a-b).** The fracture surface is sharp, revealing its weak resistance to crack

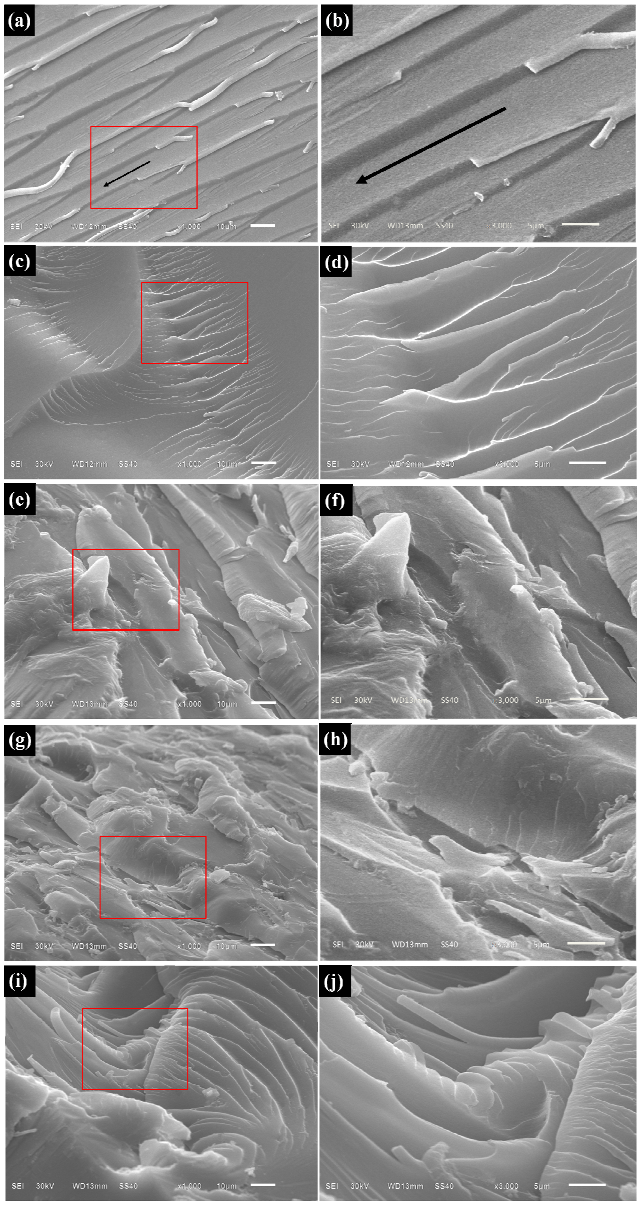


**Fig. 4** SEM images of fractured surface of composites with different enlargement fraction: (a, b) neat epoxy, (c, d) 0.5 wt%, (e, f) 1.0 wt%, (g, h) 1.5 wt%, (i, j) 2.0 wt%.

initiation, propagation and extension resistance [16]. This indicates the fracture of the neat epoxy resin is a typical brittle fracture. However, the modified epoxy composite exhibits tough fracture as shown in **Fig. 4(c-i)**. Comparing to the neat epoxy, the crack propagation direction is scattered and the fracture surface is rough and irregularity. With increasing magnification, more river line, toughening nest and wavy notch can be seen clearly. The evidence to prove crack deflection occurring is that fracture energy increased due to the presence of localized shear yielding around particles and some contribution of the crack-pinning mechanism [44]. Moreover, the degree of tough fracture reduces after increasing along with the increment of the H20-g-PDI content. Sleek fracture section can absorb fracture energy to hinder crack propagation [44]. In addition, the H20-g-PDI filler has vast hydroxyl-terminated, which react with epoxy group in epoxy resin. However, the fracture surface becomes angular and sharp when the filler content exceed 1.5 wt% leading to agglomerates [45]. It plays an important role on tough fracture of the material. There are more toughening nest and indentations than that of the neat epoxy, indicating the typical characteristic of toughening facture.

### 3.3. Mechanical properties of composites

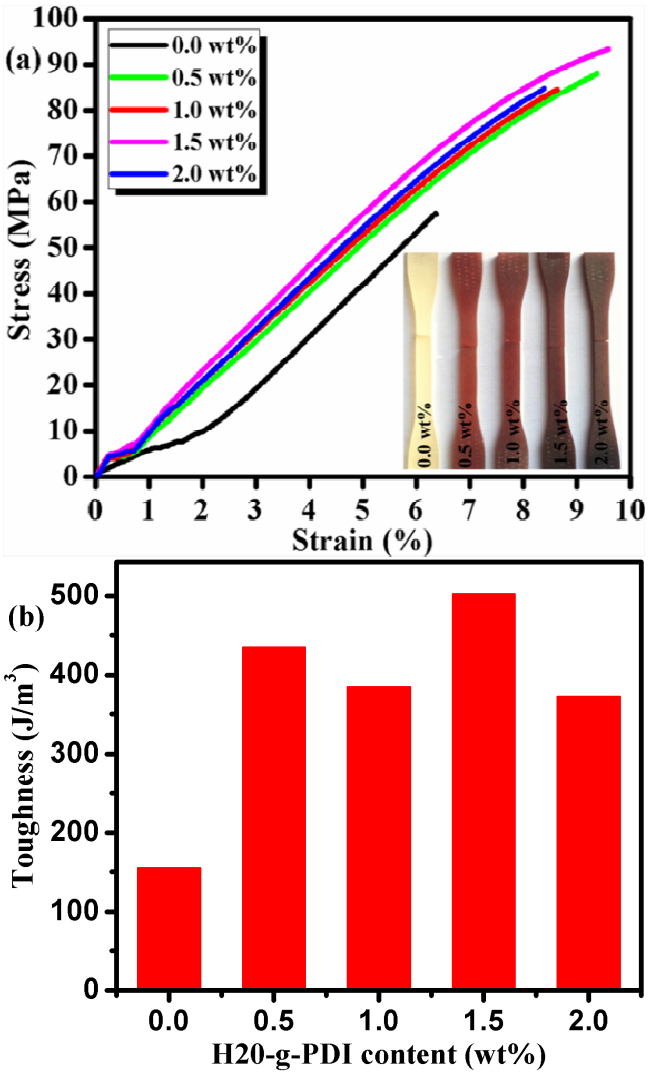


**Fig. 5** Typical stress-strain curves (a) and toughness of the epoxy composites (b).

The stress-strain curves and toughness of neat epoxy and its composites with different contents are shown in **Fig. 5**. As can be seen from **Fig. 5(a)**, the trend of the curves is similar to linear right up to the fracture breaking point, without plastic deformation [46], and the tensile strength is related to the filler contents. It is obvious that epoxy composites added a small amount of H20-g-PDI has a significant influence on the mechanical behavior. However, tensile performance declines when the filler content is over 1.5 wt%. The toughness (area under stress-strain curve) of the neat epoxy and epoxy composites are shown in the **Fig. 5(b)**. The toughness of epoxy composites was improved extremely comparing to that of neat epoxy. Hence, the properties of epoxy composites with 1.5 wt% H20-g-PDI reached maximum value. The toughness of the epoxy composite with 1.5 wt% H20-g-PDI was 502.71 J/m$^3$, which

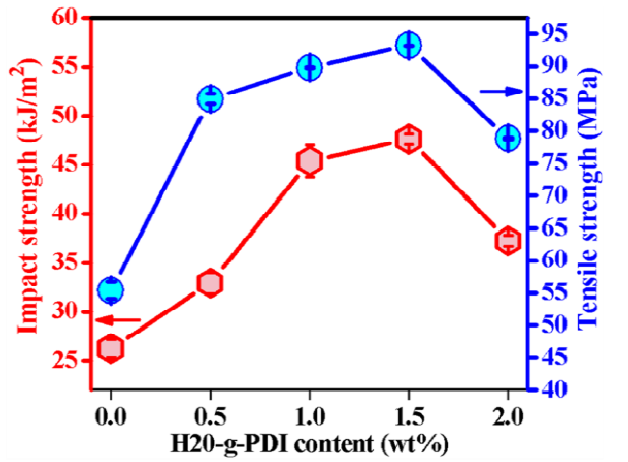


**Fig. 6** Impact strength and tensile strength of the neat epoxy and its composites.

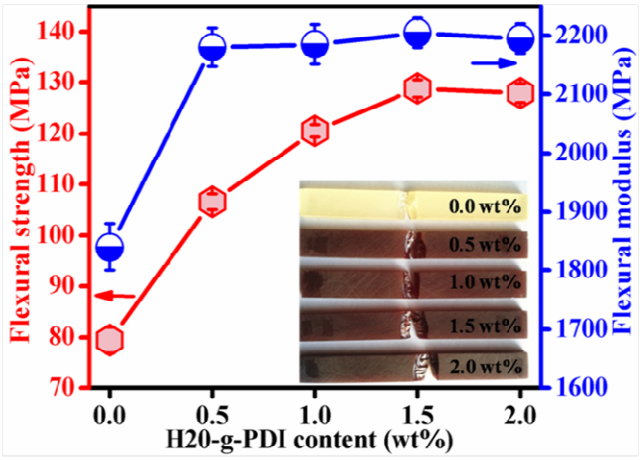


**Fig. 7** Flexural strength and modulus of the neat epoxy and its composite.

increases by 224.02 % corresponding to neat epoxy resin (155.15 J/m$^3$). Comparing neat epoxy to different content composites, the variations of impact strength and tensile strength are shown in **Fig. 6**. As can be seen from it, the impact strength and tensile strength of the compounds are obviously improved. The impact strength and tensile strength of the cured epoxy resins increases with increment of the H20-g-PDI content, that is to say, the filler content of 1.5 wt% has the maximum value according to the **Fig. 6**. When H20-g-PDI content is up to 1.5 wt%, the impact strength (47.60 KJ/m$^2$) and tensile strength (93.19 MPa) of the composite material are higher than that of neat epoxy resin by 81.33% (26.25 KJ/m$^2$) and 68.12% (55.43 MPa), respectively. The reason of this phenomenon shows three aspects as follows: Firstly, this is attributed to the reaction between epoxy groups in epoxy resin and hydroxyl groups attaching to the surface of the H20-g-PDI, which contributes to improve the toughness of epoxy resin composites. Secondly, the formed network structure can take more mechanical loading from the matrix when the matrix is under stress [14]. However, the mechanical properties of composites are expected to undergoes a slight decay if the filler content exceed 1.5 wt%. Because the dispersion of filler in the epoxy resin becomes worse with increment content of H20-g-PDI, which may induce epoxy matrix yielding phase separation and result in a defect in the epoxy matrix [34]. Finally, the stereo-hindrance effect of the H20-g-PDI would become prominent and suppressed hydrogen bonding, thus the impact strength would be deteriorated [47].

**Fig. 7** shows the flexural properties of the neat epoxy and epoxy composites. The results also show an improvement in flexural strength and modulus of the modified compounds compared to that of neat epoxy. This is attributed to the stronger interfacial adhesion between epoxy matrix and H20-g-PDI and PDI possesses rigid benzene ring structure [48]. The flexural strength values of the different content composite range from 106.60 MPa to 128.80 MPa, which are much higher than that of neat epoxy (79.50 MPa). The change trend of the flexural modulus is similar to flexural strength curve, which range from 2180 MPa to 2205 MPa. And the values of composites were higher than that of the neat epoxy (1840 MPa).The flexural strength and flexural modulus of epoxy composites with 1.5 wt% H20-g-PDI content reach the maximum values, which is 128.80 MPa and 2205 MPa, respectively. However, the flexural properties of the epoxy composites decreased, Once the filler content was exceed 1.5 wt%. That was because of the particle loading exceeds the critical level, named mechanical percolation [49]. The excess particles are poor dispersion in the epoxy, which result in agglomerates in the polymer matrix, induce cracks fracture easily and reduces fracture energy of the composites [50]. The mechanical properties of epoxy composites are attributed to form the strong covalent bonding via the hydroxyl groups of the H20-g-PDI and epoxy group of the epoxy resin and have good dispersion in epoxy matrix [51]. **Table 2** summarizes the mechanical properties data.

**Table 2** The mechanical properties of neat epoxy and its composites.

| H20-g-PDI content | Impact strength (KJ/m$^2$) | Tensile strength (MPa) | Flexural strength (MPa) | Flexural modulus (MPa) |
|---|---|---|---|---|
| 0.0 wt% | 26.25±0.90 | 55.43±1.33 | 79.50±2.50 | 1840±40 |
| 0.5 wt% | 32.91±1.08 | 89.78±0.08 | 106.60±1.52 | 2180±33 |
| 1.0 wt% | 45.37±1.65 | 84.96±0.74 | 120.55±0.20 | 2185±34 |
| 1.5 wt% | 47.60±0.56 | 93.19±0.08 | 128.80±1.69 | 2205±25 |
| 2.0 wt% | 37.24±0.57 | 78.87±0.11 | 127.90±1.82 | 2195±25 |

### 3.4 Thermal properties of composites

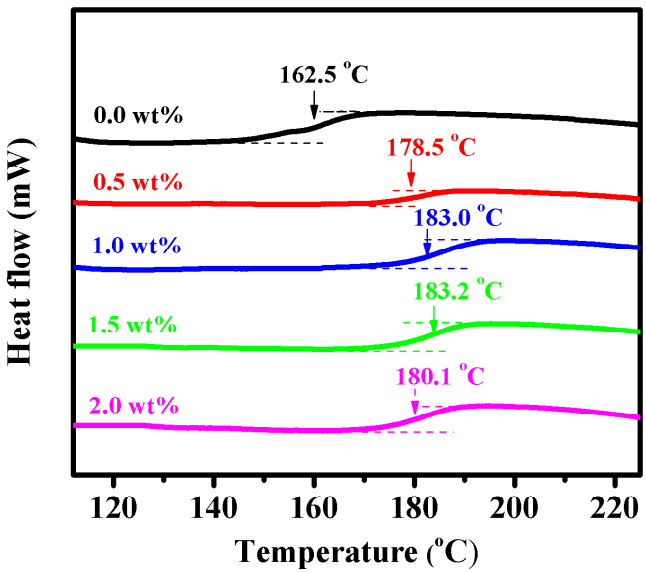


**Fig. 8** DSC curves of the neat epoxy and its composites.

**Fig. 8** exhibits the DSC curves of neat epoxy and its composites. The glass transition temperature ($T_g$) range is obtained by DSC testing. It

can be seen that the $T_g$ of neat epoxy is about 162.5 °C. The epoxy composites exhibit higher $T_g$ in comparison with that of neat epoxy. The $T_g$ increases up to the maximum value when filler content is 1.5 wt% and then decreases afterwards. The maximum value is about 183.2 °C, which increases by 20.7 °C. The $T_g$ depends on many factors, such as chain flexibility, cross-linking, intermolecular attraction and steric effects. Firstly, the H20-g-PDI has a rigid benzene ring plane structure. So it enhances $T_g$ of the epoxy composites [52]. Secondly, the matrix and chemical groups on the filler's surface may participate in the curing reaction, leading to the higher crosslinking density. The surface of the H20-g-PDI has large number of hydrogen bonds, leading to the increase of the intermolecular attraction and restricted of the composites' mobility [10]. And the hyperbranched structure of H20 molecules has large steric effects, which can also increase $T_g$ of the composites [20]. However, when the excessive amount of H20-g-PDI is introduced into the neat epoxy resin, $T_g$ is reduced to some degree because flexible polymer chains can decrease cross-linking density and lead to increase free volume for molecular relaxation [53].

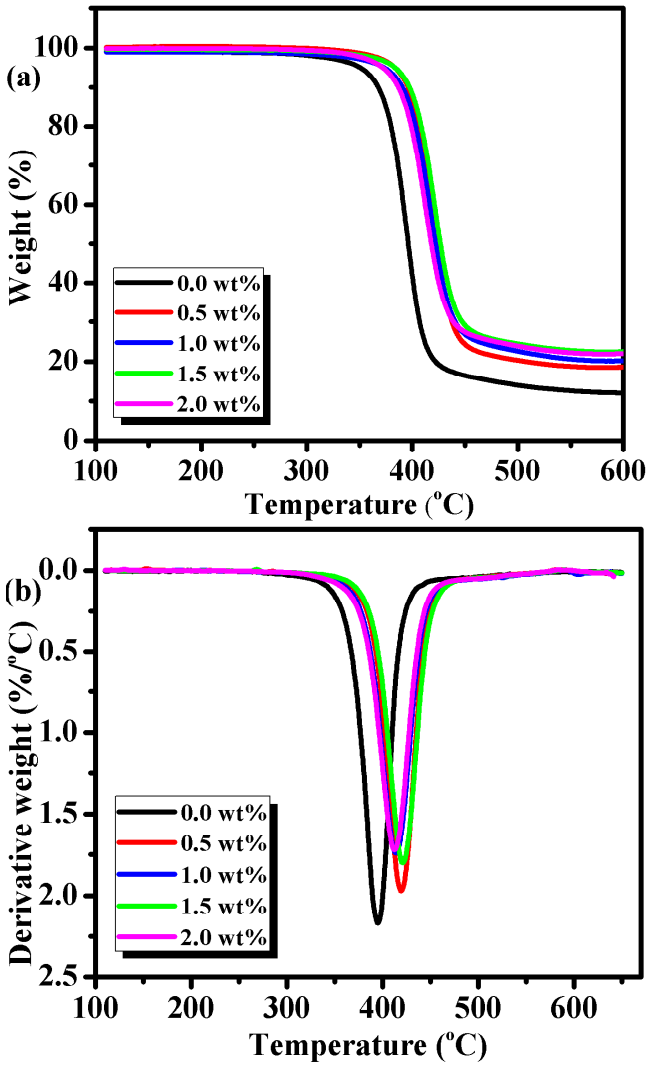


**Fig. 9** TGA (a) and DTG (b) curves of the neat epoxy and its composites.

**Fig. 9** shows the TGA and DTG curves for neat epoxy and its composites at a heating rate of 10 °C/min in nitrogen. As can be seen from the curves, all samples exhibit the similar thermal decomposition behavior. It suggests that the degradation mechanism of the epoxy composites unchange by the addition of H20-g-PDI [54]. In addition, decomposition temperatures and char yield of the composites are higher than that of neat epoxy. It can be seen that the epoxy composite of 1.5 wt% H20-g-PDI has the maximum char yield (24.22%). This is attributed to that the increased crosslinking density can limit the mobility of epoxy resin molecular chains [55]. Meanwhile, the maximal decomposition temperature of the epoxy increases from 394.61 °C to 421.56 °C, which almost increases 27 °C comparing to the neat epoxy. Thus it can conclude that the addition of H20-g-PDI improve the thermal property of epoxy composites. The decomposition temperature increase firstly then decrease after the content over 1.5 wt% H20-g-PDI. Moreover, it is apparently seen from the DTG curves that the composite has the maximum degradation temperature (421.56 °C) when the content of H20-g-PDI is 1.5 wt%. The initial decomposition temperatures ($T_i$) and the maximal decomposition temperature ($T_{max}$) are listed in the **Table 3**. The improvement of thermal stabilities can be attributed to the hyperbranched structure of the composite, which has many voids. So it can rotate and result in the twisted path for the volatile degradation substance, which delays thermal decomposition behavior [52]. Another reason is the crosslinking reaction between the hydroxyl of the surface of the H20-g-PDI and the epoxy groups of epoxy, which has the effect of the space isolation and restrict of the thermal motion [56].

**Table 3** Thermal stability of the composites calculated from TGA curves.

| The content of H20-g-PDI | Initial decomposition temperature ($T_i$) | Temperature at weight loss of 50% ($T_{50}$) | Maximum decomposition temperature ($T_{max}$) | Char yield at 550 °C (%) |
|---|---|---|---|---|
| 0.0 wt% | 331.82 | 395.74 | 394.61 | 11.47 |
| 0.5 wt% | 375.39 | 423.83 | 419.06 | 17.14 |
| 1.0 wt% | 360.34 | 422.34 | 412.54 | 18.77 |
| 1.5 wt% | 374.66 | 426.82 | 421.56 | 24.22 |
| 2.0 wt% | 361.07 | 417.86 | 411.78 | 20.32 |

**Fig. 10** displays the variations in storage modulus and tan δ of neat epoxy and its' composites. The test temperature ranges from 45 °C to 250 °C, which is below the glassy state temperature and then reaching the rubbery plateau of epoxy composites. The storage modulus reveals the amount of elastic energy stored in the composite, which is correlated to the mechanical properties and the interfacial interaction [57]. As shown in **Fig. 10(a)**, the storage modulus of the neat epoxy is higher than other compositions at glassy state region. Because this temperature provides sufficient energy to undergo conformation transition and promotes chain segment motion of neat epoxy [54]. In contrast, there was a strong effect of H20-g-PDI fillers in the rubbery region at elevated temperature where the improvement in the elastic properties of epoxy composites was clearly observed. For instance, the storage modulus of epoxy composition containing 1.5 wt% filler and neat epoxy were 1462.08 MPa and 865.91 MPa at 140 °C, which exceed 68.85%. The change in the rubbery plateau is attributed to the degree of cross-linking, chains mobility and free volume of the composites, etc. On one hand, the surfaces of H20-g-PDI and epoxy resin contain hydroxyl and epoxy group, respectively, which can promote the cross-linking reaction to reach the goal of increasing the storage modulus [58]. On the other hand, the degree of cross-linking and the hyperbranched structure of H20 damp the motion of chain segment and reduce free volume of the composite materials [59]. The storage modulus of the materials increases as the addition the H20-g-PDI. However, the storage modulus decreases when filler content is

exceed 1.5 wt%, which indicates that the filler content exceeds optimal level due to agglomerates of the excess filler particles. **Fig. 10(b)** shows that tanδ value of neat epoxy and its' composites. The DMA testing makes the $T_g$ more accurate. The $T_g$ of neat epoxy was 163.59 °C. However, the $T_g$ value increased to 192.16 °C with the increment of filler, which increased nearly 29 °C. This can be explained that the crosslink density is one of most important factors influencing on $T_g$. And free volume of the composites was reduced with adding the H20-g-PDI, which decreased the mobility of the chain segment [59]. Thereby it improved the thermal stability of the composite materials. From the **Fig. 10(b)** can be seen, $T_g$ is almost at the same without changing with the increment of content, indicating epoxy compositions form a stable network structure. Thus it suggests thermodynamic performance of epoxy resin can be modified by H20-g-PDI, which is in agreement with DSC results [57].

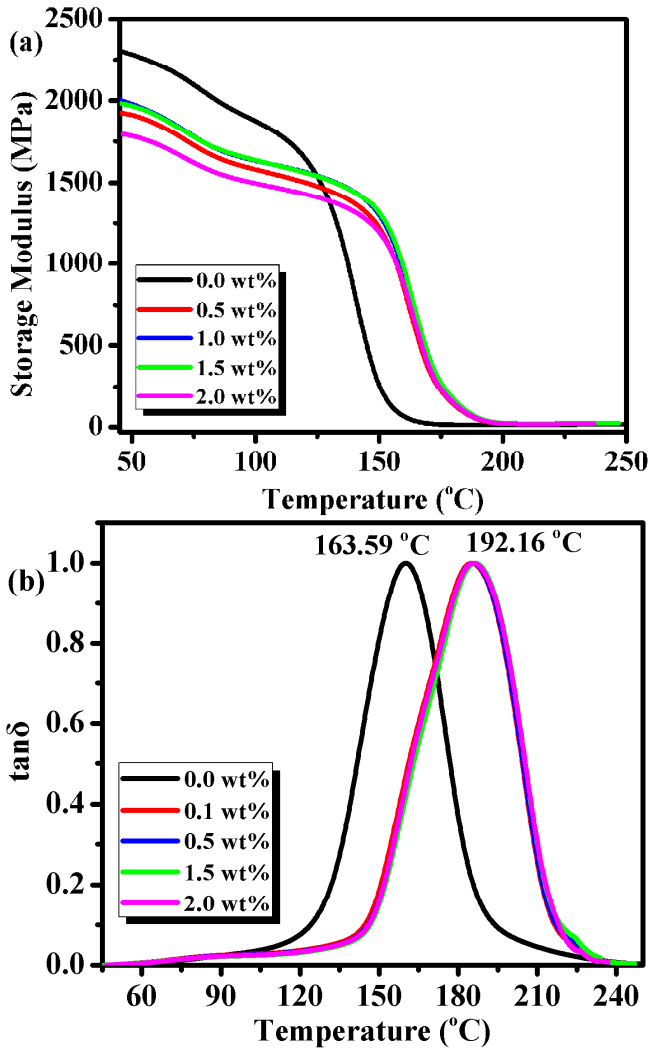


**Fig. 10** Storage modulus (a) and tanδ (b) of neat epoxy and its' composites.

## 4. Conclusions

The H20-g-PDI was synthesized successfully and incorporated into epoxy matrix. The effect of H20-g-PDI on the mechanical and thermal properties of epoxy composites was investigated. The results show that H20-g-PDI/epoxy enhances the thermal and mechanical properties. For instance, the impact strength, tensile strength, flexural strength and flexural modulus of the composites with 1.5 wt% H20-g-PDI were 47.6 KJ/m$^2$, 93.19 MPa, 128.8 MPa, and 2205 MPa. Compared to that of neat epoxy, these values represent improvements of 81.33%, 68.1%, 62.0%, and 19.8%, respectively, compared to that of neat epoxy. Moreover, the addition of H20-g-PDI produced composites with higher thermal degradation temperatures and glass transition temperatures of epoxy composites. On the basis of our work, it can provide new functional materials of epoxy composites, which is of great importance for both fundamental research and real applications.

## Acknowledgements

The authors gratefully acknowledge the financial support by National Natural Science Foundation of China (51163004, 51463007 and 51303034), the Natural Science Foundation of Guangxi Province, China (2013GXNSFAA019308, 2014GXNSFDA118006 and 2014GXNSFBA118034), Guangxi Universities Scientific Research Project (No. YB2014165), Natural Science Foundation of Ningbo (No.Y40307DB05), Guangxi Small Highland Innovation Team of Talents in Colleges and Universities and Guangxi Funds for Specially-appointed Expert.

## References

1 F. Würthner, *Chem. Comm*., 2004, **14**, 1564-1579.
2 K. Balakrishnan, A. Datar, R. Oitker, H. Chen, J. M. Zuo and L. Zang, *J. Am. Chem. Soc.,* 2005, **127**, 10496-10497.
3 X. Q. Li, V. Stepanenko, Z. Chen, P. Prins, L. D. A. Siebbeles and F.Würthner,. *Chem. Comm.,* 2006, **37**, 3871-3873.
4 M. Han, G. C. Wang and H. Q. Duan, *Chin. Chem. Lett.,* 2013, **9**, 51-54.
5 G. Boobalan, P. M. Imran and S. Nagarajan, *Chin. Chem. Lett.,* 2012, **23**, 149-153.
6 Y. Zhuo, M. Zhao, W. J. Qiu, G. F. Gui, Y. Q. Chai and R. Yuan, *J. Electroanal Chem.,* 2013, **709**, 106-110.
7 P. Mukhopadhyay, Y. Iwashita, M. Shirakaw, S. Kawa, N. Fujita and S. Shinkai, *Angew. Chem. Int. Ed.,* 2006, **45**, 1592 -1595.
8 M. Funahashi and A. Sonoda, *Org. Electron.,* 2012, **13**, 1633-1640.
9 M. M. Shi, V. C. Tung, J. J. Nie, H. Z. Chen and Y. Yang, *Org. Electron.,* 2014, **15**, 281-285.
10 L. C. Gu, T. X. Wang, W. Zhang, G. Z. Liang, A. J. Gu and L. Yuan, *RSC Adv.,* 2013, **3**, 7071-7082.
11 C. Klinkowski, S. Wagner, M. Ciesielski and M. Döring, *Polym. Degrad. Stab.,* 2014, **106**, 122-128.
12 J. P. Patel and P. H. Parsania, *Adv. Polym. Tech.,* 2014, **33**, 21398-21402.
13 V. Joudon, G. Portemont, F. Lauro and B. Bennani, *Eng. Frac. Mechan.,* 2014, **126**, 166-177.
14 V. K. Srivastava, *Mater. Des.,* 2012, **39**, 432-436.
15 V. D. Ramosa, H. M. D. Costa, V. L. P. Soares and R. S. V. Nascimento, *Polym. Test.,* 2005, **24**, 219-226.
16 L. C. Tang, H. Zhang, S. Sprenger, L. Ye and Z. Zhang, *Compos. Sci. Technol.,* 2012, **72**, 558-565.

17 B. B. Johnsen, A. J. Kinloch, R. D. Mohammed, A. C. Taylor and S. Sprenger, *Polymer,* 2007, **48**, 530-541.
18 M. Wang, Y. F. Yu, X. G. Wu and S. J. Li, *Polymer,* 2004, **45**, 1253-1259.
19 D. M. Dhevi, A. A. Prabu, H. Kim and M. Pathak, *J. Polym. Res*., 2014, **21**, 503-511.
20 C. S. Wu, Y. L. Liu and K. Y. Hsu, *Polymer,* 2003, **44**, 565-573.
21 B. Voit, *J Polym Sci Part A: Polym. Chem*., 2000, **38**, 2505-2525.
22 H. Miao, L. L. Cheng and W. F. Shi, *Prog. Org. Coat*., 2009, **65**, 71-76.
23 J. P. Yang, Z. K. Chen, G. Yang, S. Y. Fu and L. Ye, *Polymer,* 2008, **49**, 3168-3175.
24 G. Xu, W. Shi, M. Gong, F. Yu and J. P. Feng, *Polym. Adv. Technol*., 2004, **15**, 639-644.
25 F. L. Jin and S. J. Park, *J. Polym. Sci. Part B: Polym. Phys*., 2006, **44**, 3348-3356.
26 I. B. G. Cicala, C. L. Faro, O. Motta and G. Recca, *Polym. Eng. Sci.,* 2006, **46**, 1502-1511.
27 A. Houel, J. Galy, A. Charlot and J. F. Gérard, *J. Appl. Polym. Sci.,* 2014, **131**, 39830-39838.
28 P. G. Parzuchowski, M. Kizlinska and G. Rokicki, *Polymer,* 2007, **48**, 1857-1865.
29 M. Sangermano, G. Malucelli, R. Bongiovanni, A. Priola and A. Harden, *Polym. Int.,* 2005, **54**, 917-921.
30 S. R. Lu, C. Wei and X. W. Yang, *Trans. Nonferrous. Met. Soc. China.,* 2006, **16**, 665-670.
31 L. Boogh, B. Pettersson and J. A. E. Manson, *Polymer,* 1999, **40**, 2249-2261.
32 D. J. Lee, J. S. Kong and H. D. Kim, *Fiber. Polym.,* 2000, **1**, 12-17.
33 S. N. Jaisankar, D. J. Nelson and C. N. Brammer, *Polymer*, 2009, **50**, 4775-4780.
34 S. R. Lu, Y. M. Jiang and C. Wei, *J. Mater. Sci.,* 2009, **44**, 4047-4055.
35 B. Das, U. Konwar, M. Mandal and N. Karak, *Ind. Crop. Prod*., 2013, **44**, 396-404.
36 H. Icil and S. Icli, *J. Polym. Sci. Part A: Polym. Chem.,* 1997, **35**, 2137-2142.
37 K. P. Chen, X. J. Yu, C. R. Tian and J. H. Wang, *Energy. Convers. Manage.,* 2014, **77**, 13-21.
38 J. P. Yang, Z. K. Chen, G. Yang, S. Y. Fu and L. Ye, *Polymer,* 2008, **49**, 3168-3175.
39 H. Wu, J. Xu, Y. Liu and P. Heiden, *J. Appl. Polym. Sci.,* 1999, **72**, 151-163.
40 Z. J. Chen, M. G. Debije, T. Debaerdemaeker, P. Osswald and F. Würthner, *Chem. Phys. Chem.,* 2004, **5**, 137-140.
41 M. G. Debije, Z. J. Chen, J. Piris, R. B. Neder, M. M. Watson and K. Mullen, *J. Mater. Chem.,* 2005, **15**,1270-1276..
42 F. Würthner, C. Thalacker, S. Diele and C. Tschierske, *Chem. Eur. J*., 2001, **7**, 2245-2253.
43 Q. P. Feng, X. J. Shen, J. P. Yang, S. Y. Fu, Y. W. Mai and K. Friedrich, *Polymer,* 2011, **52**, 6037-6045.
44 K. H. Ding, G. L. Wang and M. Zhang, *Mater. Des.,* 2011, **32**, 3986-3991.
45 S. B. Chen, Q. H. Wang and T. M. Wang, *Mater. Des.,* 2012,**38**, 47-52.
46 X. E. Xiao, S. R. Lu, B. Qi, C. Zeng, Z. K. Yuan and J. H. Yu, *RSC Adv.,* 2014, **4**, 14928-14935.
47 T. Raju, Y. M. Ding, Y. L. He, L. Yang, M. Paula and W. M. Yang, *Polymer*, 2008, **49**, 278-294.
48 Y. Q. Li, R. Umer, A. Isakovic, Y. A. Samad, L. X. Zheng and K. Liao, *RSC Adv.,* 2013, **3**, 8849-8856.
49 J. Dong, C. Q. Yin, X. Zhao, Y. Z. Li and Q. H. Zhang, *Polymer,* 2013, **54**, 6415-6424.
50 B. Qi, S. R. Lu, X. E. Xiao, L. L. Pan, F. Z. Tan and J. H. Yu, *Express. Polym. Lett.,* 2014, **8**, 467-479.
51 M. T. Bashar, U. Sundararaj and P. Mertiny, *Polym. Eng. Sci.,* 2014, **54**, 1047-1055.
52 X. Wu, Y. Wang, L. Xie, J. Yu, F. Liu and P. Jiang, *Iran. Polym. J.,* 2013, **22**, 61-73.
53 D. M. Dhevi, S. N. Jaisankar and M. Pathak, *Eur. Polym. J.,* 2013, **49**, 3561-3572.
54 L. J. Luo, Y. Meng, T. Qiu and X. Y. Li, *J. Appl. Polym. Sci.,* 2013, **130**, 1064-1073.
55 H. W. He, K. X. Li, J. Wang, G. H. Sun, Y. Q. Li and J. L. Wang, *Mater. Des.,* 2011, **32**, 4521-4527.
56 Z. K. Yuan, J. H. Yu, B. L. Rao, H. Bai, N. Jiang and J. Gao, *Macromol. Res.,* 2014, **22**, 405-411.
57 S. H. Hsu, M. C. Wu, S. Chen, C. M. Chuang, S. H. Lin and W. F. Su, *Carbon,* 2012, **50**, 896-905.
58 D. Zhou, H. Wang, S. Wang, D. Liu and Y. Lian, *J. Appl. Polym. Sci.,* 2011, **123**, 1147-1152.
59 H. Sun, Y. Liu, H. Tan and X. Du, *J. Appl. Polym. Sci*., 2014, **131**, 39882-39888.